Improved thermoelectric performance in p-type $Bi_{0.48}Sb_{1.52}Te_3$ bulk material by adding $MnSb_2Se_4$*

Binglei Cao(曹丙垒)[1,2], Jikang Jian(简基康)[1,†], Binghui Ge(葛炳辉)[2], Shanming Li(李善明)[2], Hao Wang(王浩)[2], Jiao Liu(刘骄)[1], Huaizhou Zhao(赵怀周)[2,‡]

[1] *Physics and Optoelectronics Engineering College, Guangdong University of Technology, Guangzhou* 510006, *China*
[2] *Beijing National Laboratory for Condensed Matter Physics, Institute of Physics, Chinese Academy of Sciences, Beijing* 100190, *China*

(Received 13 September 2016; revised manuscript received 26 October 2016; published online 22 December 2016)

Bismuth telluride (Bi_2Te_3) based alloys, such as p-type $Bi_{0.5}Sb_{1.5}Te_3$, have been leading candidates for near room temperature thermoelectric applications. In this study, $Bi_{0.48}Sb_{1.52}Te_3$ bulk materials with $MnSb_2Se_4$ were prepared using high-energy ball milling and spark plasma sintering (SPS) process. The addition of $MnSb_2Se_4$ to $Bi_{0.48}Sb_{1.52}Te_3$ increased the hole concentration while slightly decreasing the Seebeck coefficient, thus optimising the electrical transport properties of the bulk material. In addition, the second phases of $MnSb_2Se_4$ and $Bi_{0.48}Sb_{1.52}Te_3$ were observed in the $Bi_{0.48}Sb_{1.52}Te_3$ matrix. The nanoparticles in the semi-coherent second phase of $MnSb_2Se_4$ behaved as scattering centres for phonons, yielding a reduction in the lattice thermal conductivity. Substantial enhancement of the figure of merit, ZT, has been achieved for $Bi_{0.48}Sb_{1.52}Te_3$ by adding an $Mn_{0.8}Cu_{0.2}Sb_2Se_4$ (2 mol%) sample, for a wide range of temperatures, with a peak value of 1.43 at 375 K, corresponding to $\sim 40\%$ improvement over its $Bi_{0.48}Sb_{1.52}Te_3$ counterpart. Such enhancement of the thermoelectric (TE) performance of p-type Bi_2Te_3 based materials is believed to be advantageous for practical applications.

Keywords: $Bi_{0.48}Sb_{1.52}Te_3$, thermoelectric materials, semi-coherent second phase, ZT enhancement

PACS: 72.15.JF, 74.25.fg **DOI:** 10.1088/1674-1056/26/1/017202

1. Introduction

Direct heat-electricity conversion is an important research topic. In particular, thermoelectrics (TE) have attracted increasing attention owing to its significant potential applicability in waste heat harvesting and cooling applications.[1–5] Thermoelectric materials utilize the Seebeck effect to generate electricity from heat sources, and their performance is determined by the dimensionless figure of merit $ZT = S^2T/[\rho(K_L + K_e)]$, where S, ρ, K_L, K_e, and T are the Seebeck coefficient, electrical resistivity, lattice thermal conductivity, electrical thermal conductivity, and absolute temperature, respectively. Ideally, enhancement of ZT for a TE material can be achieved by reducing the material's thermal conductivity and improving its power factor, which is defined as $PF = S^2/\rho$.[6]

As classical thermoelectric materials with a near room temperature TE energy conversion, Bi_2Te_3 and its alloys have been extensively studied since the 1950s. Recently, it was suggested that the performance of Bi_2Te_3 based alloys could be further improved. Till now, two approaches have been used for improving the thermoelectric properties of these materials. The first approach involves optimising the sample preparation process. For instance, Kim *et al.*[7] confirmed that the peak ZT value of $Bi_{0.5}Sb_{1.5}Te_3$ could be increased to 1.86 ± 0.15 at 320 K owing to the increased phonon scattering by dislocation at the grain boundary of bulk materials. Xie *et al.* reported a high ZT of 1.56 in $Bi_{0.52}Sb_{1.48}Te_3$ alloys using melt spinning.[8] Zheng *et al.* obtained a ZT of 1.22 for $Bi_{0.5}Sb_{1.5}Te_3$ via plasma-activated sintering (MSPAS) at 340 K.[9] An early breakthrough was reported for nanostructured BiSbTe alloys, for which a ZT of 1.4 was obtained at 373 K by ball milling and hot pressing.[10] The second approach involves the use of composites. Qin *et al.* increased the peak ZT value to 1.6 at 476 K by adding Cu_3SbSe_4 to $Bi_{0.4}Sb_{1.6}Te_3$.[11] Li *et al.* reported enhanced ZT performance in $Bi_{0.3}Sb_{1.7}Te_3$ accompanied by a significantly improved mechanical strength, following the addition of SiC nanoparticles.[12] The above results reveal a rich potential for further improving the TE performance of Bi_2Te_3-based alloys by tuning the alloy composition and microstructure.

In this study, we achieved substantial enhancement of the TE performance of $Bi_{0.48}Sb_{1.52}Te_3$ alloys by adding $MnSb_2Se_4$-based materials during a combination of ball milling and hot pressing. The performance improved by $\sim 40\%$ compared with the undoped sample. $MnSb_2Se_4$ has been identified as an intrinsic p-type semiconductor with an energy band gap of ~ 0.31 eV, featuring a high Seebeck coefficient and low lattice thermal conductivity.[13] Based on our results, we propose that $MnSb_2Se_4$ is decomposed during the composite's fabrication, with the decomposition products acting as dopants or secondary phases to affect the thermoelectric properties of $Bi_{0.48}Sb_{1.52}Te_3$. We observed that Cu doping on Mn sites could substantially promote electric trans-

*Project supported by the National Natural Science Foundation of China (Grant Nos. 51472052 and Y6J1421A41).
†Corresponding author. E-mail: jianjikang@126.com
‡Corresponding author. E-mail: hzhao@iphy.ac.cn
© 2017 Chinese Physical Society and IOP Publishing Ltd

port and ZT.[14] Here, via the composition with $MnSb_2Se_4$ or $Mn_{0.8}Cu_{0.2}Sb_2Se_4$ during the synthesis, the optimal carrier concentration was reached and lattice thermal conductivity was reduced, enhancing the thermoelectric performance of $Bi_{0.48}Sb_{1.52}Te_3$ in a broad range of temperatures.

2. Experimental methods

The $Bi_{0.48}Sb_{1.52}Te_3/MnSb_2Se_4$ composites were prepared by mechanical alloying (MA) and spark plasma sintering (SPS). In a typical run, an individual element (Bi,99.99%; Sb,99.999%; Te,99.99% in purity) was firstly loaded into a stainless steel jar and milled for 8 h in the presence of Ar. Then, $MnSb_2Se_4$ (obtained in our previous work[14]) was added into the jar and milled for 1 h, and the obtained powder was put into a graphite die (diameter, 12.7 mm) and pressed at 673 K for 5 min under 45 MPa. In a similar approach, $Bi_{0.48}Sb_{1.52}Te_3$ composites were obtained by adding $Mn_{0.8}Cu_{0.2}Sb_2Se_4$ (obtained in our previous work[14]).

The phase structure of the as-prepared samples was analysed using x-ray diffraction (XRD) operated under 40 kV and 40 mA at room temperature using Cu Kα radiation (λ = 1.5418 Å). The microstructures of the samples were examined using scanning electron microscopy (SEM, XL30S-FFG) on the samples' cross sections, and transmission electron microscopy (TEM, Tecnai F20) specimens of the mixed BiSbTe alloys were prepared by dicing, polishing, and ion-milling. The room-temperature carrier concentration and mobility of the samples were measured using the van der Pauw technique under a reversible magnetic field of 0.5 T, using pressure-assisted W electrodes on a Nanometrics Hall measurement system with the uncertainty of $\pm 5\%$ for the Hall coefficient data. The electrical resistivity and the Seebeck coefficients of the samples were measured using a Linseis LSR-3 in the presence of high-purity He. These samples were cut into 10 mm × 3 mm × 2 mm bars, and the measurement's deviation was $\pm 5\%$. The thermal conductivities of the samples were calculated as $K = DC_pd$, where D is the thermal diffusivity, C_p is the heat capacity, and d is the measured density based on the Archimedes drainage method. All of the samples for the thermal diffusivity tests were cut into 12.7-mm-diameter and 2-mm-thickness discs, and then coated with amorphous C. The thermal diffusivities (D) were measured using Linseis XFA 500 in the presence of high-purity He.

3. Results and discussion

3.1. Structure and composition analysis

Figure 1(a) shows the XRD patterns of $Bi_{0.48}Sb_{1.52}Te_3$ obtained after adding X mol% of $MnSb_2Se_4$ (from (a) to (e), X = 0, 1, 2, 3, and 4), and those of $Bi_{0.48}Sb_{1.52}Te_3$, obtained by adding 2 mol% of $Mn_{0.8}Cu_{0.2}Sb_2Se_4$ (Fig. 1(a), trace (f)). As seen from the XRD patterns, the XRD diffraction patterns for the doped samples are identical to that of the $Bi_{0.48}Sb_{1.52}Te_3$ phase, and no secondary phases of $MnSb_2Se_4$ or $Mn_{0.8}Cu_{0.2}Sb_2Se_4$ were detected using our equipment. Meanwhile, some Mn and Se atoms form MnSe alloys in the

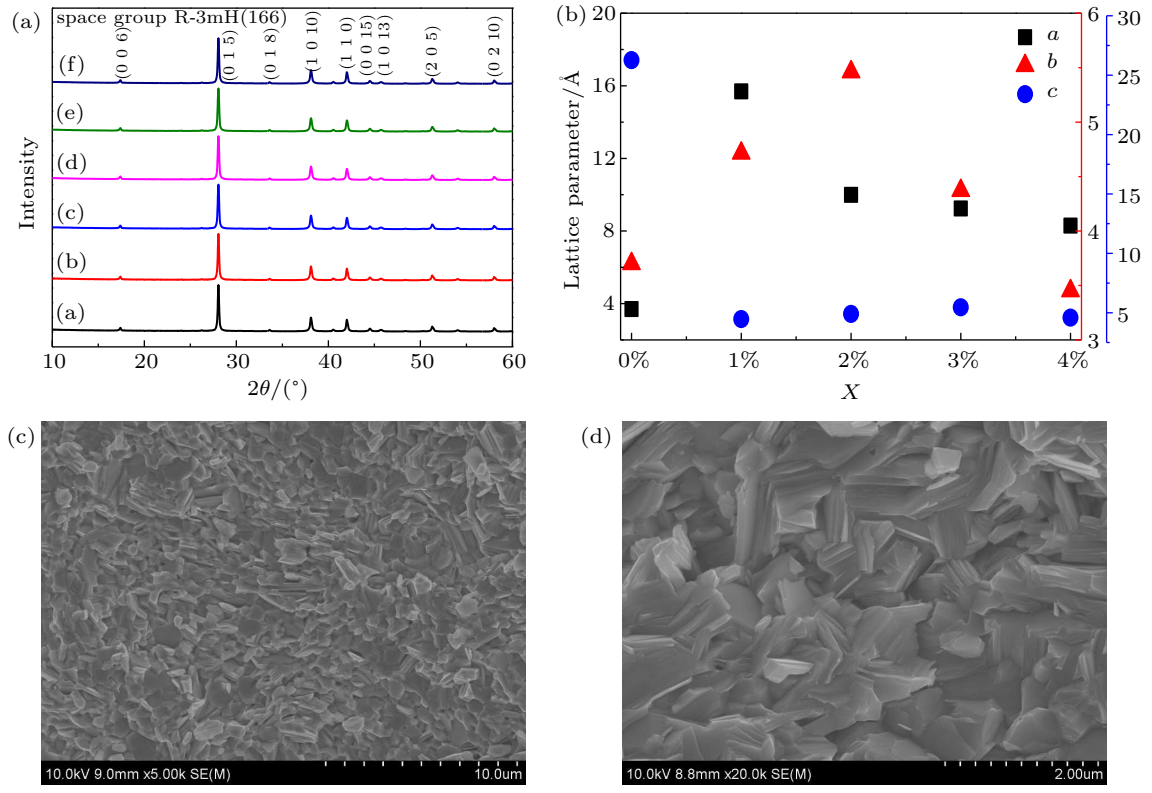


Fig. 1. (color online) (a) XRD patterns for composites $Bi_{0.48}Sb_{1.52}Te_3$ obtained by adding X mol% of $MnSb_2Se_4$ (from (a) to (e): X = 0, 1, 2, 3, and 4; (f): X = 2 $Mn_{0.8}Cu_{0.2}Sb_2Se_4$). (b) Lattice parameters (a, b, c) of $Bi_{0.48}Sb_{1.52}Te_3$ composites, obtained by adding X mol% of $MnSb_2Se_4$. (c), (d) The low- and high-magnification SEM images of doped $Bi_{0.48}Sb_{1.52}Te_3$ (obtained by adding 2 mol% of $MnSb_2Se_4$).

host, but this cannot be resolved by XRD owing to its trivial volume ratio in the composite. The above speculation is further supported by TEM images shown below. The XRD pattern of $Bi_{0.48}Sb_{1.52}Te_3$ can be indexed by the space group of R-3mH (No. 166). Figure 1(b) shows the lattice parameters (a, b, c) of the doped $Bi_{0.48}Sb_{1.52}Te_3$, as a function of the $MnSb_2Se_4$ content, for various X. Doping of the $Bi_{0.48}Sb_{1.52}Te_3$ samples increased the values of the a and b lattice parameters, compared with the undoped sample, while the values of the c lattice parameter was reduced. Meanwhile, the cell volume was reduced by the doping. Figures 1(c) and 1(d) show the low- and high-magnification SEM images of the doped $Bi_{0.48}Sb_{1.52}Te_3$ (by adding 2 mol% of $MnSb_2Se_4$), respectively, indicating that the sample exhibits uniform-size grain and no preferred texture.

Figure 2 shows the TEM and EDX images of $Bi_{0.48}Sb_{1.52}Te_3$ with added 2 mol% of $MnSb_2Se_4$ (Figs. 2(a1)–2(a3)) and 2 mol% of $Mn_{0.8}Cu_{0.2}Sb_2Se_4$ (Figs. 2(b1)–2(b3)), respectively. The low-magnification TEM image of $Bi_{0.48}Sb_{1.52}Te_3$ with $MnSb_2Se_4$ (Fig. 2(a1)) reveals uniformly sized grains and a second phase at the grain boundary, which is more clearly revealed in the amplified TEM image in Fig. 2(a2). The corresponding EDX mapping images of Bi, Sb, Te, Mn, and Se are shown in the right column in Figs. 2(a1)–2(a3). It can be seen that Bi is abundantly present at the grain boundary, which arises owing to the

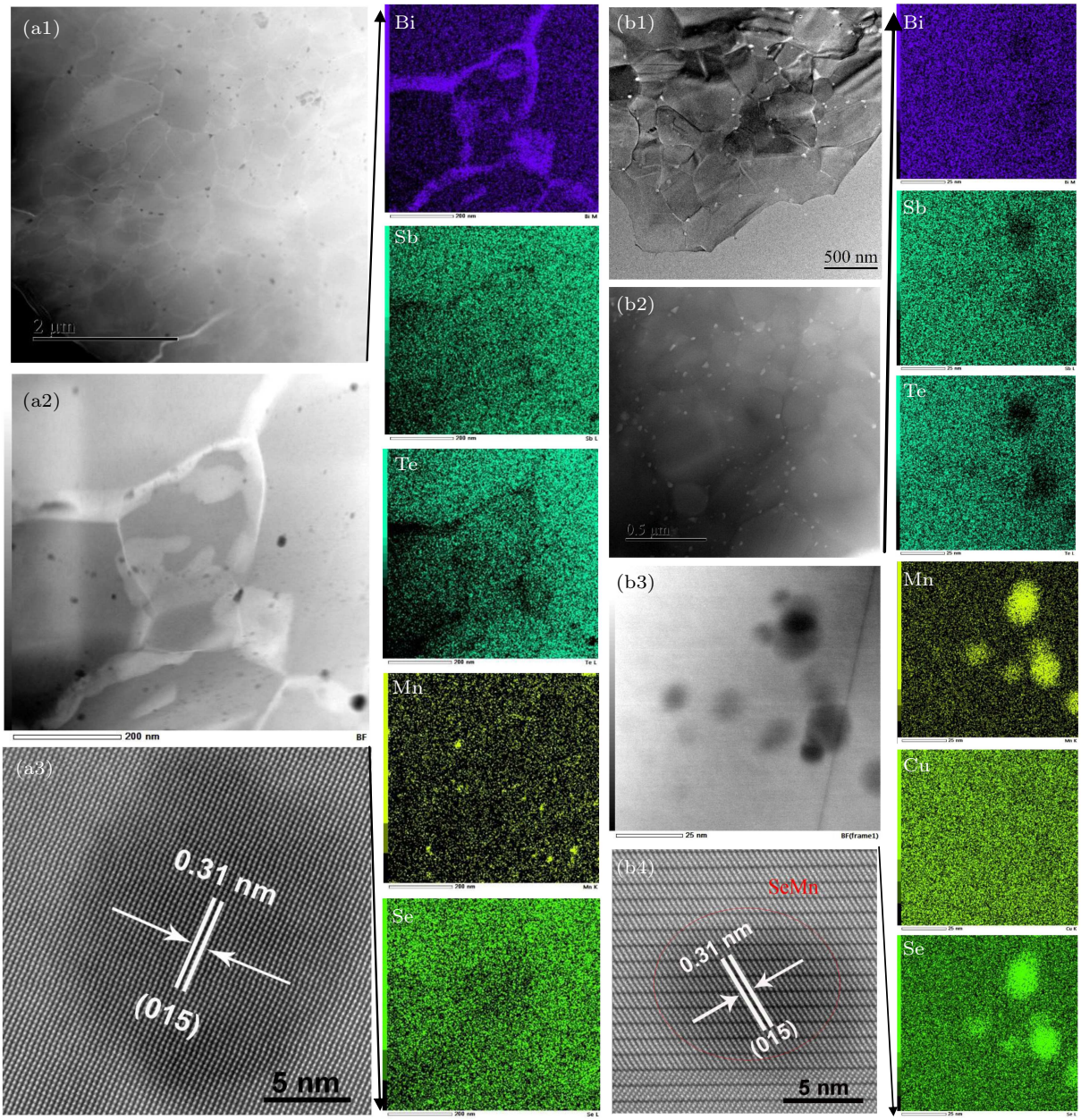


Fig. 2. (color online) Transmission electron microscopy (TEM) and energy dispersion x-ray spectrometry (EDX) mapping images of $Bi_{0.48}Sb_{1.52}Te_3$ with 2 mol% of $MnSb_2Se_4$ (column A) and with 2 mol% of $Mn_{0.8}Cu_{0.2}Sb_2Se_4$ (column B), respectively. (a1) a low-magnification TEM image of the sample, with the main body as $Bi_{0.48}Sb_{1.52}Te_3$ and the black spot corresponding to the second phase; (a2) a grain boundary TEM image of the sample; (a3) a HRTEM image of the sample matrix, the images on the right side of TEM graphs are the EDS mapping of areas in panel (a2). (b1, b2) low-magnification TEM images of the sample, with the main phase as $Bi_{0.48}Sb_{1.52}Te_3$ and the spot corresponding to the second phase; (b3) a high-magnification TEM image of the sample; (b4) a HRTEM image of the sample matrix, with the images on the right side of the TEM images showing the EDS mapping images of the area in panel (b3).

decomposition of a small amount of $Bi_{0.48}Sb_{1.52}Te_3$ in the presence of hightemperature and high pressure. Elemental Bi is in the liquid form and is expelled to the grain boundary. Figure 2(a3) shows an HRTEM image of $Bi_{0.48}Sb_{1.52}Te_3$ with 2 mol% of $MnSb_2Se_4$. In the image, the calculated inter-planar distance is ~ 0.31 nm, which is consistent with the (015) plane of $Bi_{0.5}Sb_{1.5}Te_3$ (JCPDS 49-1713).

Figures 2(b1)–2(b4) shows the microstructural features of $Bi_{0.48}Sb_{1.52}Te_3$ with 2 mol% of $Mn_{0.8}Cu_{0.2}Sb_2Se_4$. The grains are uniformly sized, and the second phase of nanoparticles is clear, too. This is more clearly revealed by the magnified TEM images in Figs. 2(b2) and 2(b3). The elemental EDX mapping in Fig. 2(b3) is shown in the left column. Cu, Sb, and Te were all uniformly distributed in the host matrix. However, Mn and Se were enriched in nanoparticles, suggesting the formation of the MnSe foreign phase. Figure 2(b4) shows a high-magnification TEM image of the sample, with a clearly identifiable lattice structure of MnSe. We suggest that alloying or replacing reactions occur in these samples. We assume that addition of $MnSb_2Se_4$ or $Mn_{0.8}Cu_{0.2}Sb_2Se_4$ to the composites results in the decomposition during the preparation process, following which Mn atoms can be incorporated into the $BiSb_2Te_3$ lattice by replacing the atoms at BiSb sites, with Se atoms replacing Te atoms, leading to the formation of the $(BiSbMn)_2(TeSe)_3$ alloy with the same lattice structure as that of $(BiSb)_2Te_3$. The EDX and HRTEM results indicate that MnSe nanoparticles emerge as the foreign second phase in the host matrix of $Bi_{0.48}Sb_{1.52}Te_3$.

3.2. Thermal and electrical transport properties

The temperature dependence of thermal conductivity, for temperatures in the 300–550 K range, for a series of samples, is shown in Fig. 3 (the data reported by Poudel *et al.* are provided for comparison[10]). As shown in Fig. 3(a), the overall thermal conductivity increases with increasing temperature. It is clear that all thermal conductivities of the doped samples are higher than that of $Bi_{0.48}Sb_{1.52}Te_3$ for temperatures under 400 K, which can be rationalised by considering their higher electrical thermal conductivities, shown in Fig. 3(c). The thermal conductivities of the composite samples are lower than that of the undoped $Bi_{0.48}Sb_{1.52}Te_3$ for $T > \sim 400$ K. The addition of $MnSb_2Se_4$ or $Mn_{0.8}Cu_{0.2}Sb_2Se_4$ increases the carrier concentration and suppresses the bipolar diffusion.[15] Figure 3(b) shows the Lorenz numbers L of the samples, which were calculated using a single parabolic band model (SPB),[16–19] as follows:[20]

$$L = 1.5 + \exp\left[-\frac{|S|}{116}\right], \tag{1}$$

where L is in 10^{-8} W·Ω·K^{-2} and S is in μV/K. Figures 3(c) and 3(d) show the temperature dependence of electrical thermal conductivities and lattice conductivities for the samples. The carrier thermal conductivity K_e can be obtained by using the Wiedemann–Franz law, $K_e = L\sigma T$, and the lattice thermal conductivity K_L can be calculated by subtracting K_e from the overall thermal conductivity K_{tot} (where L, σ, and T are the Lorenz number, the electrical conductivity, and the

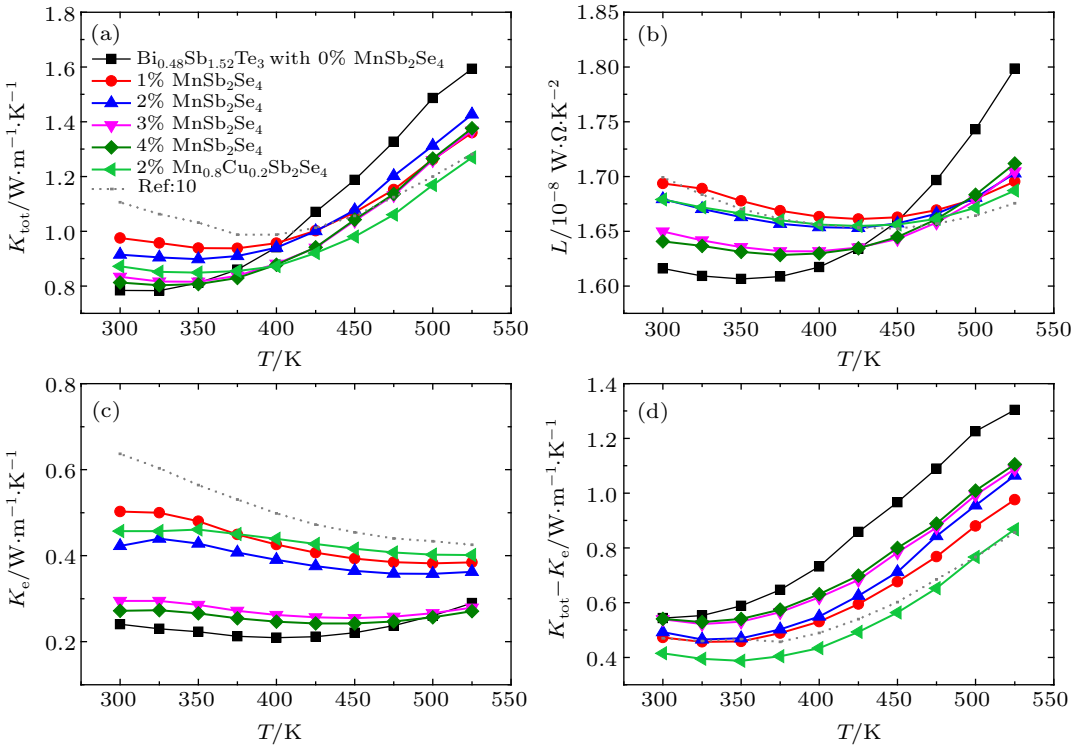


Fig. 3. (color online) Temperature dependence of (a) overall thermal conductivity K_{tot}, (b) the Lorenz number L, (c) carrier thermal conductivity K_e, (d) lattice and bipolar contributions of thermal conductivity (K_{tot}–K_e) for $Bi_{0.48}Sb_{1.52}Te_3$ with X mol% of $MnSb_2Se_4$ ($X = 0$, 1, 2, 3, and 4), 2 mol% of $Mn_{0.8}Cu_{0.2}Sb_2Se_4$ samples, and the reference nano-crystalline BiSbTe sample.[10]

temperature, respectively). Figure 3(c) shows that the K_e values for the doped samples are higher than for the $Bi_{0.48}Sb_{1.52}Te_3$, owing to the improvement in the carrier concentration. Nevertheless, the lattice thermal conductivities for the doped samples are lower than that for the undoped sample. This is mainly owing to the increased scattering from the second phase and the increased presence of structural defects in the host matrix,[21,22] as shown in Fig. 3(d). The overall thermal conductivities for the $Bi_{0.48}Sb_{1.52}Te_3$ alloys with $MnSb_2Se_4$ or $Mn_{0.8}Cu_{0.2}Sb_2Se_4$ are lower than that of the nano-crystalline BiSbTe sample below 400 K, as reported by Poudel *et al*.

Figure 4 shows the temperature dependence of the electrical resistivity ρ, the Seebeck coefficient S, the power factor PF, the ZT value, the room temperature Hall carrier concentration (n), and the carrier mobility (μ), respectively. As shown above, the electrical resistivities of the doped samples are lower than that of the undoped $Bi_{0.48}Sb_{1.52}Te_3$ sample. The can be ascribed to the substitution of Bi^{3+} by Mn^{2+} in $MnSb_2Se_4$ that contributed free vacancies, which is similar to Djieutedjeu's report.[23] The doping process can be described as follows:

$$x\mathrm{Bi}^{3+} \xrightarrow{x\mathrm{Mn}^{2+}} x\mathrm{Mn}'_{\mathrm{Bi}} + \chi h^{*}. \tag{2}$$

In addition, the lowest electrical resistivity was achieved for $Bi_{0.48}Sb_{1.52}Te_3$ with 2 mol% of $Mn_{0.8}Cu_{0.2}Sb_2Se_4$. This can also be ascribed to the substitution of Bi^{3+} by Cu^{+}, resulting

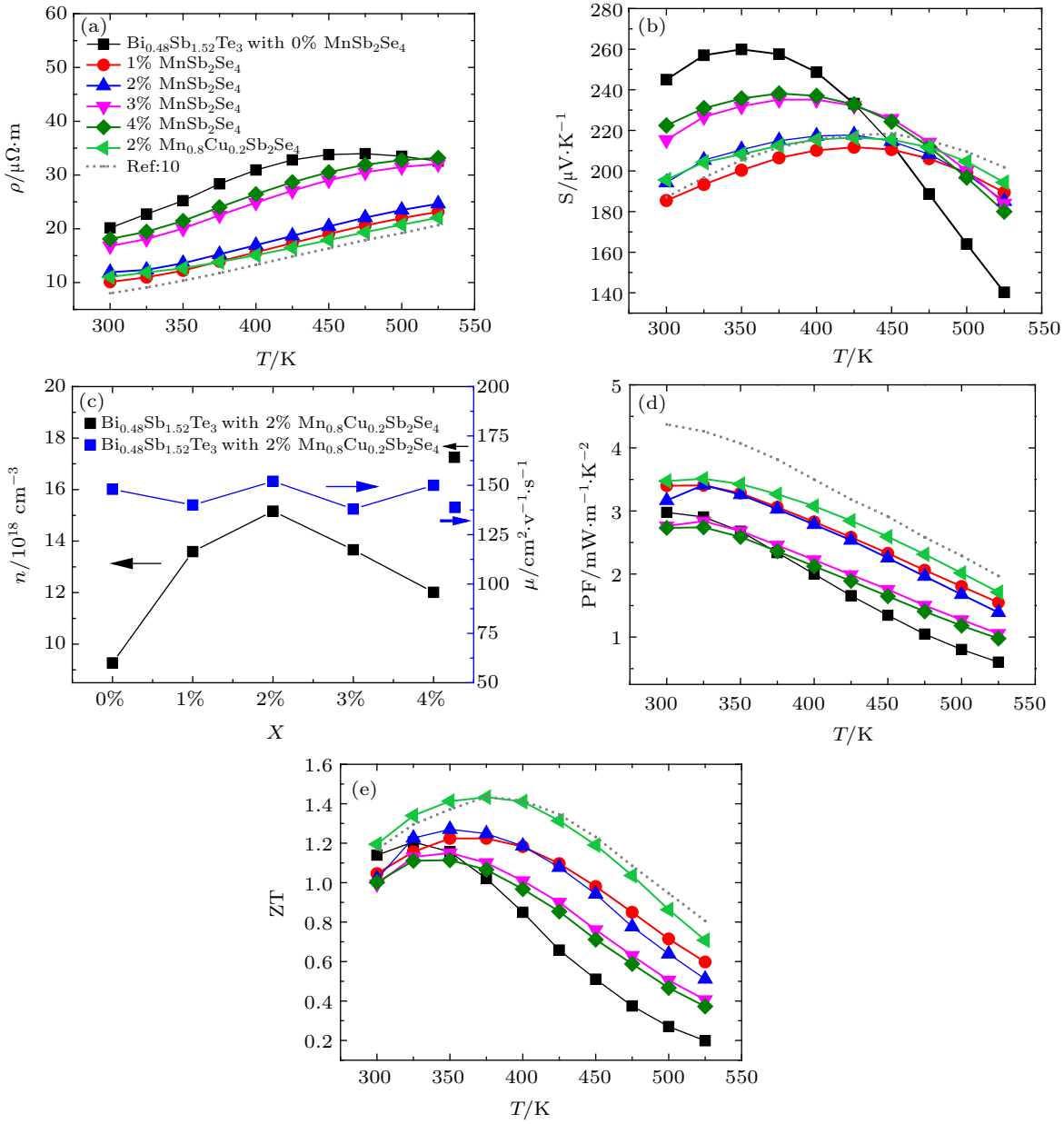


Fig. 4. (color online) Temperature dependence of (a) the electrical resistivity ρ, (b) the Seebeck coefficient S, (d) the power factor PF, (e) the ZT value for $Bi_{0.48}Sb_{1.52}Te_3$ samples with X mol% of $MnSb_2Se_4$ ($X = 0$, 1, 2, 3, and 4), with 2 mol% of $Mn_{0.8}Cu_{0.2}Sb_2Se_4$, and for the nano-crystalline BiSbTe reference sample.[10] (c) Room-temperature Hall carrier concentration (n) and carrier mobility (μ) for the $Bi_{0.48}Sb_{1.52}Te_3$ samples with various amount of $MnSb_2Se_4$ ($X = 0$, 1, 2, 3, and 4), and the independent data for a 2 mol% $Mn_{0.8}Cu_{0.2}Sb_2Se_4$ sample.

in two more free vacancies in the sample. This process can be described as follows:

$$y\mathrm{Bi}^{3+} \xrightarrow{y\mathrm{Cu}^{+}} y\mathrm{Cu}''_{\mathrm{Bi}} + 2yh^{*}. \quad (3)$$

Thus, it is expected that the carrier concentration in the $Bi_{0.48}Sb_{1.52}Te_3$ sample doped with $Mn_{0.8}Cu_{0.2}Sb_2Se_4$ is higher than those in other samples, which is supported by the data in Fig. 4(c). From Fig. 4(b), the Seebeck coefficients of the doped samples are lower than that of the undoped sample below 450 K, and the Seebeck coefficient of the undoped $Bi_{0.48}Sb_{1.52}Te_3$ decreases faster than those of other samples with increasing the temperature, and this may be owing to the increasing hole concentrations for the doped samples, as shown in Fig. 4(c). Figure 4(c) shows the room temperature Hall carrier concentration and carrier mobility for the samples (the independent points of different carrier concentrations and carrier mobility represent $Bi_{0.48}Sb_{1.52}Te_3$ with 2 mol% of $Mn_{0.8}Cu_{0.2}Sb_2Se_4$). The reference $Bi_{0.48}Sb_{1.52}Te_3$ exhibits a low carrier concentration ($n \sim 9.27 \times 10^{18}$ cm^{-3}), while the carrier concentration increases with the addition of $MnSb_2Se_4$. The highest carrier concentration is obtained after adding 2 mol% of $MnSb_2Se_4$ ($n \sim 15.16 \times 10^{18}$ cm^{-3}), and the highest carrier mobility ($\mu \sim 152$ cm^2·V^{-1}·s^{-1}) is achieved for the same sample. The carrier concentration for $Bi_{0.48}Sb_{1.52}Te_3$ with 2 mol% of $Mn_{0.8}Cu_{0.2}Sb_2Se_4$ reaches a maximum of $\sim 17.52 \times 10^{18}$ cm^{-3} and the carrier mobility is 140 cm^2·V^{-1}·s^{-1}. However, the hole mobility is weakly dependent on the amount of $MnSb_2Se_4$, as shown in Fig. 4(c), because the hole moves close to the Te position, but Mn and Cu substitute for the Bi position and therefore cause weak scattering at the hole.[24]

Figure 4(d) shows the power factors (PF) of all samples, and it is obvious that the power factors of all of the doped samples are improved. The PF of $Bi_{0.48}Sb_{1.52}Te_3$ with 2 mol% of $Mn_{0.8}Cu_{0.2}Sb_2Se_4$ is higher than others, constituting an average $\sim 20\%$ improvement over that of the undoped $Bi_{0.48}Sb_{1.52}Te_3$. Owing to a high electrical resistivity, the power factor of the sample with 2 mol% of $Mn_{0.8}Cu_{0.2}Sb_2Se_4$ is lower than that of the nano-crystalline (NC) BiSbTe sample.[10] Figure 4(e) shows the temperature-dependent ZTs of the samples, revealing a significant improvement of the ZT values of doped samples. In particular, the ZT value for $Bi_{0.48}Sb_{1.52}Te_3$ with 2 mol% of $Mn_{0.8}Cu_{0.2}Sb_2Se_4$ is the most striking, and the maximal ZT value of ~ 1.43 at 375 K reveals a $\sim 40\%$ improvement over the value for the reference $Bi_{0.48}Sb_{1.52}Te_3$. Overall, incorporating a small quantity of $MnSb_2Se_4$ or $Mn_{0.8}Cu_{0.2}Sb_2Se_4$ into $Bi_{0.48}Sb_{1.52}Te_3$ alloys significantly improves their thermoelectric performance.

Figure 5 shows the cumulative temperature dependence of thermoelectric performance, for all samples. To evaluate the energy conversion efficiency (η) and output power density (Pd_{eng}) of the TE material, the engineering dimensionless figure of merit (ZT_{eng}) and the engineering power factor (PF_{eng}) have been developed by Kim *et al.*[26] ZT_{eng} can be expressed as follows:

$$(\mathrm{ZT})_{\mathrm{eng}} = \frac{\left(\int_{T_c}^{T_h} S(T)\,\mathrm{d}T\right)^2}{\int_{T_C}^{T_h} \rho(T)\,\mathrm{d}T \int_{T_c}^{T_h} k(T)\,\mathrm{d}T}\Delta T = \frac{(PF)_{\mathrm{eng}}}{\int_{T_c}^{T_h} k(T)\,\mathrm{d}T}\Delta T, \quad (4)$$

where T_h, T_c, and ΔT are the hot-side temperature, the cold-side temperature, and T_h–T_c, respectively. The output power density (P_d) can be obtained from the engineering power factor (PF_{eng}), as follows:[26]

$$P_{\mathrm{d}} = \frac{(\mathrm{PF})_{\mathrm{eng}}\,\Delta T m_{\mathrm{opt}}}{L\left(1+m_{\mathrm{opt}}\right)^2}, \quad (5)$$

where L is the Lorenz number and m_{opt} is defined as $m_{\mathrm{opt}} = \sqrt{1+ZT_{\mathrm{avg}}}$.

Figure 5(a) shows the dependence of ZT_{eng} on ΔT for the doped samples, clearly showing that the ZT_{eng} values of the doped samples are substantially enhanced with respect to that of the undoped sample. In particular, a ZT_{eng} value of 0.62 (at $\Delta T = 225$ K) for BiSbTe with 2 mol% of $Mn_{0.8}Cu_{0.2}Sb_2Se_4$ is higher than that for the other samples, which reveals a $\sim 60\%$ improvement over the value for the undoped sample, mostly owing to a higher PF_{eng}, as shown in Fig. 5(c). Figure 5(b) shows the energy conversion efficiency (η) for all of the samples. The cumulative temperature-dependent maximal efficiency is defined as[26]

$$\eta_{\max} = \eta_c \frac{\sqrt{1+(\mathrm{ZT})_{\mathrm{eng}}\left(\hat{a}/\eta_c - 1/2\right)} - 1}{\hat{a}\left(\sqrt{1+(\mathrm{ZT})_{\mathrm{eng}}\left(\hat{a}/\eta_c - 1/2\right)} + 1\right) - \eta_c}, \quad (6)$$

where η_c is the Carnot efficiency and $\hat{a}$ is a dimensionless intensity factor of the Thompson effect (which plays an important role in increasing the efficiency[25]) defined as

$$\hat{a} = \frac{S(T_h)\,\Delta T}{\int_{T_c}^{T_h} S(T)\,\mathrm{d}T},$$

in which $S(T_h)$ is the Seebeck coefficient at the hot-side temperature T_h. The efficiency of $Bi_{0.48}Sb_{1.52}Te_3$ with 2 mol% of $Mn_{0.8}Cu_{0.2}Sb_2Se_4$ approaches 10.24% at $\Delta T = 225$ K, which is $\sim 40\%$ higher than that of the undoped $Bi_{0.48}Se_{1.52}Te_3$ sample. Figures 5(c) and 5(d) show the engineering power factor (PF_{eng}) and the output power density (P_d), for all of the samples. The PF_{eng} and P_d for all of the doped samples have been improved, especially for the sample with $Mn_{0.8}Cu_{0.2}Sb_2Se_4$. Thus, a high value of engineering ZT_{eng} (0.62) and a high conversion efficiency (η) of 10.24% (at $\Delta T = 225$ K) were obtained for the $Bi_{0.48}Sb_{1.52}Te_3$ alloy by adding $Mn_{0.8}Cu_{0.2}Sb_2Se_4$.

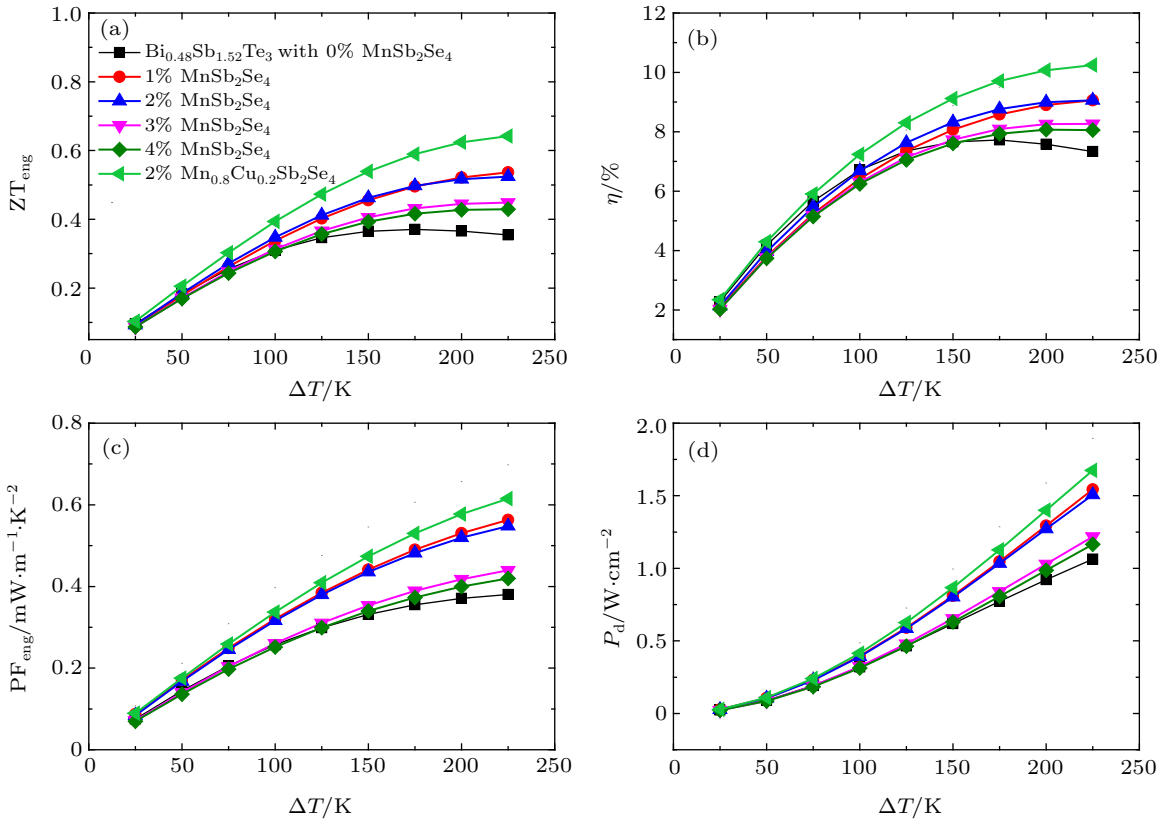


Fig. 5. (color online) Cumulative temperature dependence of (a) engineering dimensionless figure of merit $(ZT)_{eng}$, (b) energy conversion efficiency (η), (c) engineering power factor (PF_{eng}), (d) output power density (P_d).

4. Conclusions

In summary, ~40% improvement in peak ZT, from 1.02 to 1.43 at 375 K, has been achieved for p-type $Bi_{0.48}Sb_{1.52}Te_3$ by adding 2 mol% of $Mn_{0.8}Cu_{0.2}Sb_2Se_4$ during the synthesis process. The improvement of ZT can be ascribed to the increase in the power factor by optimisation of carrier concentration, and to the reduction in the lattice thermal conductivity owing to the increased phonon scattering by the foreign second phases. This study demonstrates that incorporation of $MnSb_2Se_4$ into p-type BiSbTe can enhance the thermoelectric performance of the latter.

References

[1] Liu N, Luo X G, Zhang M L 2014 *Chin. Phys. B* **23** 080502

[2] Disalvo F J 1999 *Science* **285** 703

[3] Harman T C, Taylor P J, Walsh M P and LaForge B E 2002 *Science* **297** 2229

[4] Wu S H, Ryosuke N, Masatsugu, Zhang Q S, Chihaya A 2014 *Chin. Phys. B* **23** 098502

[5] Lin T, Zeng Z H and Wang C H 2014 *Acta Phys. Sin.* **63** 197201 (in Chinese)

[6] Kaur K and Kumar R 2016 *Chin. Phys. B* **25** 026402

[7] Kim S, Lee K H, Mun H A, Kim H S, Hwang S W, Roh J W, Yang D J, Shin W H, Li X S, Lee Y H, Snyder G J and Kim S W 2015 *Science* **348** 109

[8] Xie W J, Tang X F, Yan Y G, Zhang Q J and Tritt T M 2009 *Appl. Phys. Lett.* **94** 102111

[9] Zheng Y, Zhang Q, Su X L, Xie H Y, Shu S C, Chen T L, Tan G J, Yan Y G, Tang X F, Uher C and Snyder G J 2015 *Adv. Energy Mater.* **5** 1401391

[10] Poudel B, Hao Q, Ma Y, Lan Y C, Minnich A, Yu B, Yan X, Wang D Z, Muto A, Vashaee D, Chen X Y, Liu J M, Dresslhaus M S, Chen G and Ren Z F 2008 *Science* **320** 634

[11] Li Y Y, Li D, Qin X Y, Yang X H, Liu Y F, Zhang J, Dou Y C, Song C J and Xin H X 2015 *J. Mater. Chem. C* **3** 7045

[12] Li J H, Tan Q, Li J F, Liu D W, Li F, Li Z Y, Zou M M and Wang K 2013 *Adv. Funct. Mater.* **23** 4317

[13] Djieutedjeu H, Makongo J P A, Rotaru A, Palasyuk A, Takas N J, Zhou X Y, Ranmohotti K G S, Spinu L, Uber C and Poudeu P F P 2011 *Eur. J. Inorg. Chem.* **26** 3969

[14] Li S M, Zhao H Z, Zhang H, Ren G K, Liu N, Li D D, Yang C S, Jin S F, Shang D S, Wang W H, Lin Y H, Gu L and Chen X L 2015 *RSC Adv.* **5** 99065

[15] Goldsmid H J 1965 *The Thermal Properties of Solids,* vo1. 1, (New York: Dover Publications, Inc), p. 62

[16] May A F, Toberer E S, Saramat A and Snyder G J 2009 *Phys. Rev. B* **80** 125205

[17] Shi X Y, Pei Y Z, Snyder G J and Chen L D 2011 *Energy Environ. Sci.* **4** 4086

[18] Korkosz R J, Chasapis T C, Lo S H, Doak J W, Kim Y J, Wu C I, Hatzikraniotis E, Hogan T P, Ssidman D N, Wolverton C, Dravid V P and Kanatzidis M G 2014 *J. Am. Chem. Soc.* **136** 3225

[19] Xie H H, Wang H, Pei Y Z, Fu C G, Liu X H, Snyder G J, Zhao X B and Zhu T J 2013 *Adv. Funct. Mater* **23** 5123

[20] Kim H S, Gibbs Z M, Tang Y L, Wang H and Snyder G J 2015 *Appl. Phys. Lett. Mater.* **3** 041506

[21] Ma Y, Qing H, Poudel B, Lan Y H, Yu B, Wang D Z, Chen G and Ren Z F 2008 *Nano Lett.* **8** 2580

[22] Hu L P, Zhu T J, Wang Y G, Xie H H, Zhao J X and Zhao X B 2014 *NPG Asia Mater.* **6** e88

[23] Djieutedjeu H, Zhou X Y, Chi H, Haldolaarachchige N, Ranmohotti K G S, Uber C, Young D and Poudeu P F P 2014 *J. Mater. Chem. C* **2** 6199

[24] Gao M, Zhang J Y and Rowe D M 1996 p. 71

[25] Hsiao Y Y, Chang W C and Chen S L 2010 *Energy* **35** 1447

[26] Kim H S, Liu W S, Chen G, Chu C W and Ren Z F 2015 *PNAS* **112** 8205